nature communications

Article

https://doi.org/10.1038/s41467-024-54208-y

Late-stage (radio)fluorination of alkyl phosphonates via electrophilic activation

Received: 21 May 2024

Accepted: 1 November 2024

Published online: 28 November 2024

Check for updates

Kaiqiang Zhang[1,2,3,10], Wanru Feng[1,2,3,10], Zhaobiao Mou[1,2,3,10], Lei Zhang[4], Mengting Ma[1,2,3,5], Zixiao Zhao[1,2,3], Xia Liu[1,2,3], Xiaoyuan Chen[6,7,8,9] & Zijing Li[1,2,3]

Constructing organic fluorophosphines, vital drug skeletons, through the direct fluorination of readily available alkyl phosphonates has been impeded due to the intrinsic low electrophilicity of P^V and the high bond energy of P═O bond. Here, alkyl phosphonates are electrophilically activated with triflic anhydride and *N*-heteroaromatic bases, enabling nucleophilic fluorination at room temperature to form fluorophosphines via reactive phosphine intermediates. This approach facilitates the late-stage (radio)fluorination of broad dialkyl and monoalkyl phosphonates. Monoalkyl phosphonates derived from targeted drugs, including cyclophosphamide, vortioxetine, and dihydrocholesterol, are effectively fluorinated, achieving notable yields of 47–71%. Radiofluorination of medically significant ^{18}F-tracers and synthons are completed in radiochemical conversions (radio-TLC) of 51–88% and molar activities up to 251 ± 12 GBq/μmol (initial activity 11.2 GBq) within 10 min at room temperature. Utilizing a phosphonamidic fluoride building block (BFPA), [^{18}F]BFPA-Flurpiridaz and [^{18}F]BFPA-E[c(RGDyK)]$_2$ demonstrate high-contrast target imaging, excellent pharmacokinetics, and negligible defluorination.

Organic fluorophosphines bearing a P^V–F bond are widely employed as agrochemicals[1–3], synthetic intermediates[4], catalysts[5–7], clickable moieties for phosphorus fluoride exchange (PFEx)[8], and building blocks for the development of ^{18}F-radiopharmaceuticals[9–16]. However, the preparation of these fluorophosphines are always constrained by the requirement for pre-modification of leaving groups (LGs), such as, –Cl[9,17–20], –H[21–24], electron-deficient –O/SAr[25], –SR (R = CF_3, Me)[26,27], or –OH[28–33]. Symmetrical fluorophosphines are primarily constructed with these conventional precursors that are usually unstable via multi-step synthesis from the ubiquitous alkyl phosphonates (Fig. 1a). The current direct ^{18}F-labeling through nucleophilic substitution of aryl phosphonate precursors, aimed at overcoming the low molar activity (A_m) associated with isotope exchange-based ^{18}F-labeling method[34] produces ionic ^{18}F-fluorophosphonates that hinder cell uptake and exhibit high bone affinity, limiting their bioavailability. The late-stage (radio)fluorination of broader alkyl phosphonates with a more efficient

[1]State Key Laboratory of Vaccines for Infectious Diseases, Center for Molecular Imaging and Translational Medicine, School of Public Health, Xiamen University, Xiamen, Fujian, China. [2]Xiang An Biomedicine Laboratory, School of Public Health, Xiamen University, Xiamen, Fujian, China. [3]State Key Laboratory of Molecular Vaccinology and Molecular Diagnostics, National Innovation Platform for Industry-Education Integration in Vaccine Research, Xiamen University, Xiamen, Fujian, China. [4]Tianjin Engineering Technology Center of Chemical Wastewater Source Reduction and Recycling, School of Science, Tianjin Chengjian University, Tianjin, China. [5]Department of Nuclear Medicine, Xiang'an Hospital affiliated to Xiamen University, Xiamen, Fujian, China. [6]Departments of Diagnostic Radiology, Surgery, Chemical and Biomolecular Engineering, and Biomedical Engineering, Yong Loo Lin School of Medicine and College of Design and Engineering, National University of Singapore, Singapore, Singapore. [7]Clinical Imaging Research Centre, Centre for Translational Medicine, Yong Loo Lin School of Medicine, National University of Singapore, Singapore, Singapore. [8]Nanomedicine Translational Research Program, Yong Loo Lin School of Medicine, National University of Singapore, Singapore, Singapore. [9]Institute of Molecular and Cell Biology, Agency for Science, Technology, and Research (A*STAR), 61 Biopolis Drive, Proteos, Singapore, Singapore. [10]These authors contributed equally: Kaiqiang Zhang, Wanru Feng, Zhaobiao Mou.
e-mail: zijing.li@xmu.edu.cn

https://doi.org/10.1038/s41467-024-54208-y

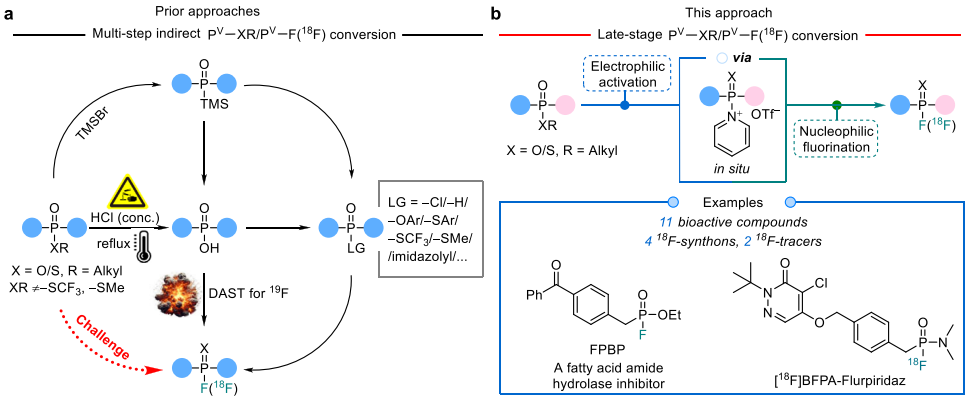

Fig. 1 | Approaches for fluorination of alkyl phosphonates. a Prior approaches rely on multi-step conversion from symmetrical alkyl phosphonates and isolation of intermediates. **b** This late-stage approach from alkyl phosphonates eliminates the requirement for hash conditions, intricate multi-step transformations and separation. OTf^- trifluoromethanesulfonate, TMSBr bromotrimethylsilane, DAST diethylaminosulfur trifluoride, Ar aryl, Me methyl. The blue and pink balls represent different substituents.

and streamlined strategy is long expected for the substantial variability of candidate structures and rapid radiosynthesis with ^{18}F[35].

Although alkyl phosphonates are susceptible to enzymolysis in vivo catalyzed by enzymes like phospholipases, synthetic methods for selective conversion of P^V–OR bond under mild conditions remains limited. The presence of p–π conjugation in alkyl phosphonates (bond dissociation energy of P=O = 585 kJ/mol) and alkyl phosphonamides significantly diminishes the electrophilicity of the P^V atom. Highly electrophilic species, such as Cu^{III} [36] and triflic anhydride (Tf_2O)[37,38], have been found to effectively activate dialkyl phosphonates through enhancing the electrophilicity of P^V. In Cu^{III}-catalyzed oxygen-arylation of dialkyl phosphonates, however, no P–X (X = coordinating atom of P) substitution occurs, in inconsistence with our expectation to form P–F bonds by replacing X. Despite the above, given that the high electronegativity of F and the small size of F^- favors the formation of π-bond with the *d*-orbital of P (pπ-dπ bonding, back-donation)[39], *N*-heteroaromatic bases may serve as active LG through an Arbuzov-like pathway, which are commonly used in Tf_2O-mediated electrophilic activation and stabilize reactive intermediates[40], allowing for broader screening options due to their various electronic substituents. Therefore, it is hypothesized that the electrophilic P^V species generated in situ by Tf_2O and *N*-heteroaromatic bases may mediate the construction of P–F bond under mild conditions (Fig. 1b).

Herein, we present a (radio)fluorination method that enables the late-stage synthesis of fluorophosphines via electrophilic activation of readily accessible alkyl phosphonates. The activation of alkyl phosphonates by diverse bases is investigated, and the effects of different fluoride sources and solvents on the fluorination yield are examined. A comprehensive series of alkyl phosphonates are rationally designed and synthesized, and the fluorination reactions of diverse phosphonates are investigated by modulating the structures of alkyl substituents. The formation and cleavage of chemical bonds during the reaction are elucidated through control experiments. Phosphorus-31 NMR spectroscopy (^{31}P NMR) and mass spectrometry (MS) are employed to monitor potential reaction intermediates in situ. In addition, density functional theory (DFT) calculations are conducted to elucidate the plausible reaction mechanism. The feasibility of late-stage fluorination of alkyl phosphonate substrates with diverse structural variations on benzyls, functional linkers and drugs is explored. The conditions and efficiency of ^{18}F-fluorination are explored based on the non-radioactive reaction conditions. Rapid preparation and positron emission tomography (PET) evaluation of medically significant ^{18}F-tracers and synthons via late-stage ^{18}F-fluorination of the corresponding alkyl phosphonate precursors are conducted for the development of PET tracers.

Results

General compounds information

In this study, the alkyl phosphonate precursors used for fluorination are designated as **S1** through **S57**, with a combination of the letter "S" and Arabic numerals. The fluorinated phosphonate products are numbered sequentially in Arabic numerals from **1** to **46**. The resulting products were fully characterized using Proton NMR spectroscopy (^1H NMR), Carbon-13 NMR spectroscopy (^{13}C NMR), Fluorine-19 NMR spectroscopy (^{19}F NMR), ^{31}P NMR and high-resolution mass spectrometry (HRMS).

Screening of bases

After optimizing the ratio of electrophilic activator and additives (Table S1), screening of *N*-heteroaromatic bases (2.0 eq.) as additives was conducted using a simple asymmetrical benzylphosphonamide monoalkyl ester (**S2**, 1.0 eq.) as the model substrate, with tetrabutylammonium fluoride (TBAF, 1.2 eq.) serving as the fluoride source in the presence of 1.5 eq. of electrophilic activator Tf_2O (Fig. 2a). It was observed that the absence of basic additives hindered the direct action of F^- on the intermediates generated from the **S2** and Tf_2O, resulting in the inability to obtain the desired fluorophosphine. Upon introducing different *N*-heteroaromatic bases into the reaction system, it was observed that pyridine (**a^1**) exhibited a higher fluorination yield of 47% compared to the other substituted pyridine additives. This could be attributed to the optimal electron cloud density of pyridine (Py), allowing it to effectively serve as both a nucleophile and a LG. In addition, imidazole (**a^5**) and 3,5-dimethylpyrazole (**a^6**) also exhibited comparable reactivity in the reaction, with **a^6** achieving the highest fluorination yield of 56%. Interestingly, ^{31}P NMR spectrum revealed that **a^6** exhibited incomplete conversion of the preceding intermediat, whereas **a^1** did. In addition to *N*-heteroaromatic bases, several common bases were also evaluated. Triethylamine (Et_3N, **a^8**) and *N*,*N*-diisopropylethylamine (DIPEA, **a^9**) were less effective due to steric hindrance, while potassium carbonate (K_2CO_3, **a^{10}**) performed poorly because of its low solubility in CH_2Cl_2. In contrast, 1,8-diazabicyclo[5.4.0]undec-7-ene (DBU, **a^{11}**) yielded 33%. Therefore, Py is considered to be the optimal *N*-heteroaromatic base.

Screening of fluoride sources

Based on the ^{31}P NMR monitoring result, the high alkalinity of TBAF (with a $pK_a > 16$ in THF)[41,42] is postulated to lead to the decomposition of intermediates and thus reduce the yield of fluorination. Consequently, various mild neutral fluoride sources were utilized in this study (Fig. 2b). NH_4F and KHF_2 were found to be almost ineffective in CH_2Cl_2 due to their limited solubility. AgF as a fluorination reagent had

https://doi.org/10.1038/s41467-024-54208-y

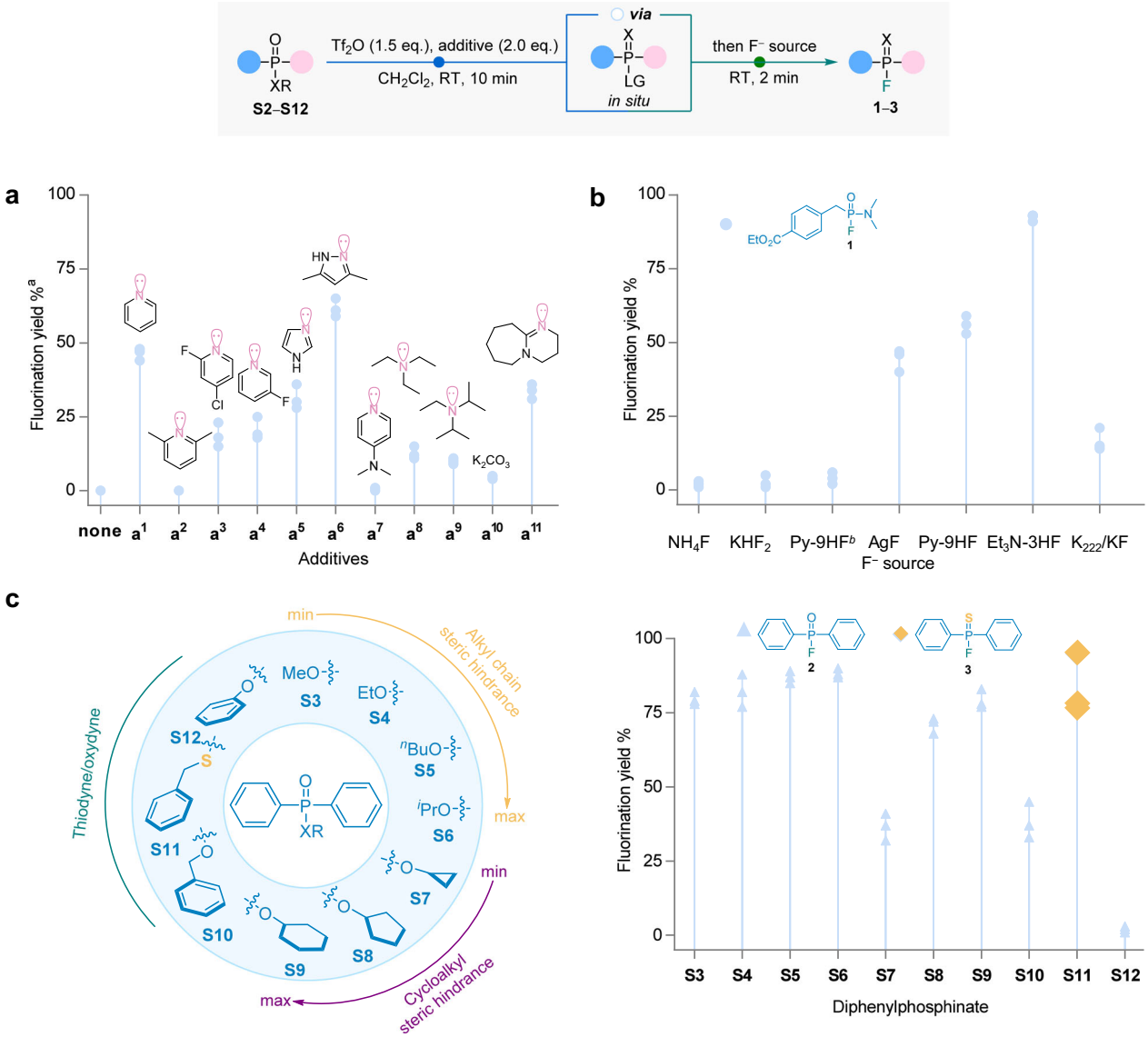

Fig. 2 | Optimization of conditions for late-stage fluorination of alkyl phosphonates via electrophilic activation. All reactions were conducted using 0.2 mmol model compounds, with a gradual addition of Tf_2O (1.5 eq., 0.3 mmol) and the additive (2.0 eq., 0.4 mmol), followed by the subsequent addition of the F^- source (1.5 eq., 0.3 mmol), in CH_2Cl_2 (1.0 mL, 0.2 M) under room temperature (RT). **a** Optimization of bases, ethyl 4-(((dimethylamino)(ethoxy)phosphoryl)methyl) benzoate (**S2**) as a model compound. [a]Yields determined by ^{31}P NMR. ^{31}P NMR was conducted by adding CD_2Cl_2 after the reaction, with the preliminary conversion proportion calculated from the ratio of product to non-product peak areas. **b** Screening of fluorine sources with **S2** as the model compound and Py as an additive. [b]No additive is added. **c**, Study of direct fluorination of different diphenylphosphonates (**S3**–**S12**).

a fluorination yield similar to TBAF of 46%, while Py-9HF as a fluorination reagent provided a slightly higher yield of 54%. Given the presence of Py in the Py-9HF complex, efforts were made to employ Py-9HF as a fluoride source without the addition of extra Py. The unsuccessful outcome of this endeavor was attributed to the notable stability of the complex under these conditions, making it challenging to liberate free Py with the necessary nucleophilic ability to engage in the reaction. Notably, $Et_3N{\cdot}3HF$ demonstrated remarkable efficacy, achieving a satisfactory fluorination yield of 92%.

Fluorination of diverse alkyl phosphonates

The reactivity of alkyl ester substituents with varying degrees of steric hindrance towards fluorination was investigated using diphenylphosphonates (**S3**–**S12**) as precursors (Fig. 2c). The results showed that substrates with varying degrees of steric hindrance had negligible impact on fluorination yields. Moreover, both cyclic and linear alkyl esters displayed effective participation in the fluorination reaction, achieving yields ranging from 32% to 90%. Interestingly, fluorination was nearly absent when phenyl diphenylphosphonate (**S12**) was used as a precursor, highlighting the high selectivity of this fluorination strategy for alkyl phosphonates. This selectivity was further confirmed by the ^{18}F-fluorination of a mixed phosphonate precursor (**S15**) substituted with −OEt and −OPh groups (see Fig. S4 for details). It is worth noting that when *S*-benzyl diphenylphosphinothioate (**S11**) was used as the precursor, the fluorination exhibited an exceptional yield of 83%, resulting in the formation of diphenylphosphinothioic fluoride **3** as the product. Consequently, this observation prompted our interest in the reaction and motivated us to explore the corresponding mechanism of fluoridation.

Mechanism

In contrast to carbonyl and sulfoxide structures, phosphorus oxides typically demonstrate reduced reactivity, thus limiting the development of their interaction with Tf_2O for electrophilic activation[43]. The

https://doi.org/10.1038/s41467-024-54208-y

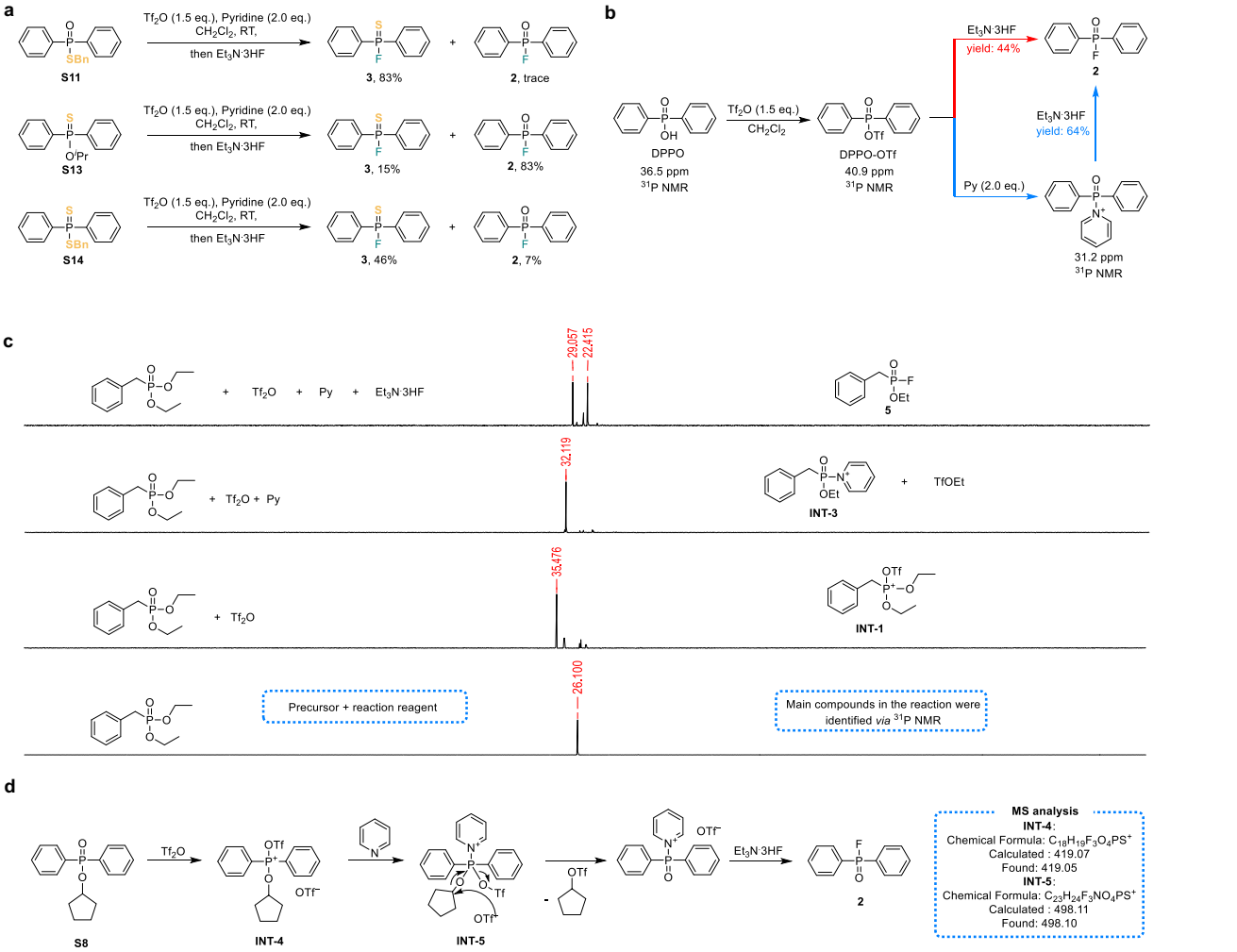

Fig. 3 | The mechanism study of late-stage fluorination of alkyl phosphonates via electrophilic activation. a Control experiment on the direct fluorination of thiophosphonic alkyl ester. **b** Control experiment of Py with diphenylphosphinic acid (DPPO) as the precursor. **c** ^{31}P NMR monitoring of stepwise reaction intermediates in situ. **d** Stepwise in situ mass spectrometric monitoring of fluorination using precursor compound **S8**.

general process of Tf_2O-mediated electrophilic activation involves the electrophilic attack of anhydrides on the electron-rich center of X=O (X = C, S, Se, P, Sb, I)[44]. This results in the cleavage of the double bond and the formation of trifluoromethyl ester intermediate (X^+), which then react and transform with nucleophilic reagents.

The foremost among our inquiries was determining whether the reaction proceeded through the direct cleavage of the P–O bond in alkyl phosphonates, resulting in the departure of –OR and facilitating the nucleophilic substitution fluorination reaction—a pivotal step in this process. To investigate the bond cleavage and formation in the reaction, control experiments using thio-precursors were conducted (Fig. 3a). In the case where **S13** served as the precursor, the primary product obtained was diphenylphosphinic fluoride **2**, accompanied by a minor quantity of diphenylphosphine thiofluoride **3**. These results clearly demonstrated that the P–O or P–S single bonds in phosphonates with P–O^{i}Pr or P–SBn groups remained intact during the fluorination of alkyl phosphonates. Instead, cleavage of the C–O or C–S bonds occurred, leading to the separation of isopropyl or benzyl segments and the formation of a new P=X bond, resembling the classical Arbuzov reaction pathway[45]. Furthermore, the aforementioned conclusion was further corroborated by the fluorination results of precursor benzyl diphenylphosphinodithioate **S14**. A method for constructing structurally diverse P=X (X = S, Se) compounds was provided, inspiring a strategy that bypasses the traditional selenization/sulfidation steps[46].

Subsequently, commercially available diethyl benzylphosphonate (**S16**) was employed as a precursor dissolved in CD_2Cl_2, successively activated with Tf_2O and Py, and then reacted with $Et_3N{\cdot}3HF$, while in situ monitoring of ^{31}P NMR was performed (Fig. 3c). Each addition of a reaction reagent resulted in a pronounced and complete shift in the ^{31}P NMR spectrum. When diethyl benzylphosphonate was incubated with Tf_2O in CD_2Cl_2 solution for 5 min, the main product exhibited a new ^{31}P NMR spectrum shift of ~35 ppm, indicating a noticeable low field movement trend. This shift was attributed to the decrease in electron cloud density at the P^+ center of the λ4σ4-phosphinic cation intermediate **INT-1**, resulting from the electrophilic activation by Tf_2O. Given that the intermediate **INT-1** cannot react with $Et_3N{\cdot}3HF$ to yield the desired product without Py, the OTf-substituted λ5σ5-type intermediate **INT-S2** was excluded (Fig. S49).

The –OTf, serving as an excellent LG, has been demonstrated to facilitate nucleophilic substitution by F^- on OTf-substituted λ5σ5-type substrate, as evidenced by the reaction of DPPO (Fig. 3b). Subsequent introduction of Py caused further shifting in the ^{31}P NMR spectrum, resulting in a single peak of ~32 ppm. Concurrently, only OTf^- and TfOEt fluorine-containing structures were identifiable in situ ^{19}F NMR (Fig. S45), the compound was inferred to be a non-fluorine-λ5σ4

https://doi.org/10.1038/s41467-024-54208-y

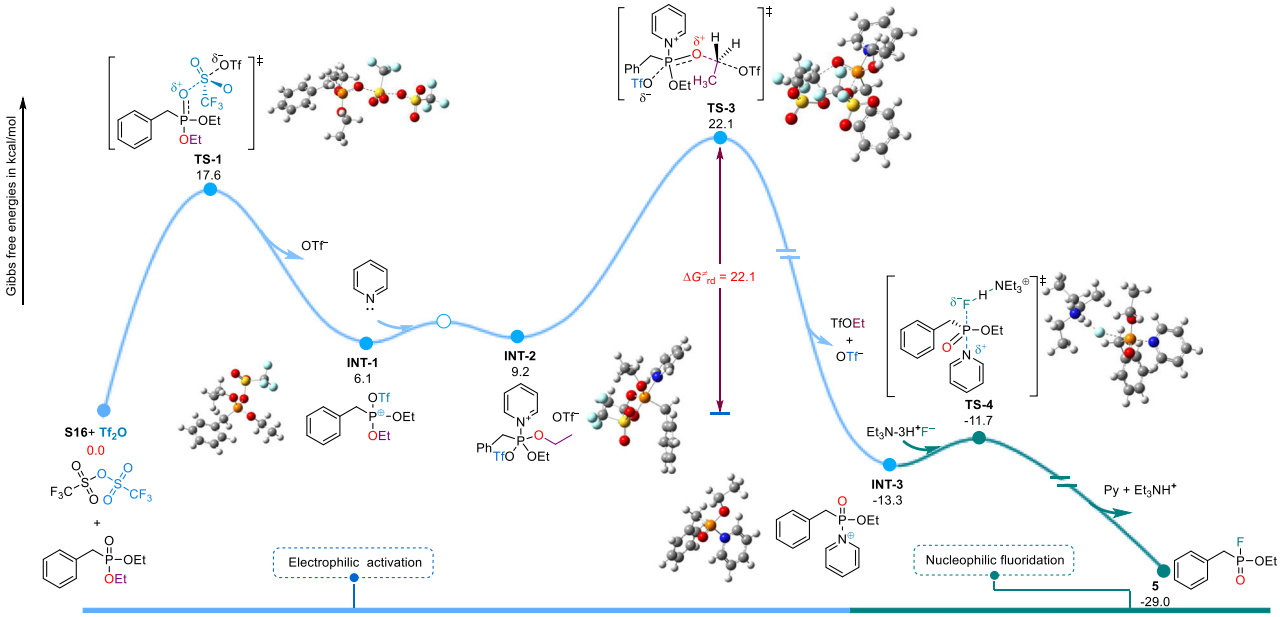

Fig. 4 | The calculated mechanism of late-stage fluorination of alkyl phosphonates via electrophilic activation. The energy distribution of alkyl phosphonate (**S16**) activated by Tf_2O for fluorination and the optimal structure of key stability points were investigated using DFT calculations. The calculated Gibbs energy (ΔG and $\Delta G^{\ddagger}_{rd}$, 298.15 K, 1.0 atm) is expressed in kcal/mol.

electrophilic phosphine-pyridinium intermediate denoted as **INT-3**. Formation of **INT-3** proceeds through two possible pathways for the departure of the ethyl fragment via Arbuzov-like processes. One route involves direct nucleophilic attack by Py on the methylene of the ester in **INT-1**, yielding the 1-ethylpyridinium byproduct with an activation barrier of 16.7 kcal/mol (Fig. S49). Another pathway involves initial interaction between Py and **INT-1** to form **INT-2**, followed by OTf^- attacking the methylene of the ester in **INT-2**, which leads to the departure of TfOEt and the formation of **INT-3**, requiring a lower activation barrier of 12.9 kcal/mol (Fig. S47). The latter pathway is energetically favored. Furthermore, in situ ^1H NMR analysis revealed that the TfOEt byproduct was ~9 times more abundant than 1-ethylpyridinium (Fig. S44)[47], supporting this mechanistic proposal. Ultimately, after $Et_3N{\cdot}3HF$ treatment, **INT-3** intermediate was nearly completely converted into fluorophosphine **5**.

Our efforts to detect these active intermediates by MS or isolate them have been unsuccessful. Nevertheless, to further support the proposed mechanistic hypothesis, cyclopentyl diphenylphosphinate (**S8**) was employed as a precursor due to the potential contributions of the diphenyl conjugated system on stabilizing certain reaction intermediates (Fig. 3d). Encouragingly, intermediates **INT-4** and **INT-5** corresponding to **INT-1** and **INT-2** were both detected through in situ MS monitoring (Fig. S46). Notably, for the first time, the possible involvement of a λ5σ5 transient intermediate in Tf_2O-mediated P=O electrophilic activation has been proposed. This insight may help in developing strategies for inducing highly stereoselective P–F compounds.

Based on experimental results, a plausible fluorination reaction mechanism is presented in Fig. 4. The change in Gibbs free energy (ΔG) for the reaction of diethyl benzylphosphonate with $Et_3N{\cdot}3HF$ to give fluorophosphine **5** was calculated by the DFT method (using the 'Gaussian 09' software; see Supplementary Information section **2.7.2**), and whether the conversion of P^V–OR to P^V–F could be thermodynamically advantageous was evaluated. The proposed fluorination process of diethyl benzylphosphinate proceeds as follows. Initially, the precursor undergoes activation by Tf_2O, resulting in the formation of the λ4σ4 P^+ intermediate **INT-1** via transition state **1** (**TS-1**). Subsequently, the **INT-1** interacts with the newly introduced Py to form intermediate **INT-2** (transition state **TS-2** has not been optimized, refer to Fig. S48). Following this, functioning as a nucleophilic reagent, OTf^- initiates an attack on the methylene of the ester, resulting in the cleavage of the C–O bond. Transitioning through **TS-3**, the λ5σ4 phosphine-pyridinium **INT-3** is generated, accompanied by the release of the byproduct TfOEt and the departure of another OTf^-. It is noteworthy that the rate-determining step of the reaction only requires crossing a barrier of 22.1 kcal/mol. Finally, through nucleophilic substitution with F^-, intermediate **INT-3** transforms into the corresponding fluorophosphine. Throughout the reaction process, which is characterized by a low energy barrier, it proceeds smoothly at room temperature (< 24 kcal/mol) and can be completed quickly and efficiently within 12 min. The entire process is spontaneous, with a total ΔG of −29 kcal/mol, indicating a strong thermodynamic driving force.

Substrate scope of alkyl phosphonates

The scope of fluorination for alkyl phosphonates was investigated, as illustrated in Fig. 5. Initially, commercially available diethyl benzylphosphonates bearing halogen substituents on the benzyl, such as −F, −Cl, −Br, and −I (**6**–**9**) exhibited excellent yields ranging from 76% to 91%. Substrates with strong electron-withdrawing groups such as $-NO_2$ or −CN (**10, 11, 16, 19, 20**) and electron-donating groups such as −Me or −OMe (**12**–**15, 18**) were well-tolerated. The conversions of ortho-substituted substrates with $-NO_2$ and −CN decreased to 51% (**19**) and 60% (**20**), respectively, likely due to increased steric hindrance. Notably, the substrate with a $-COCH_3$ substituent required specific conditions—Tf_2O (3.0 eq.) and pyridine (4.0 eq.)—to successfully yield the desired fluorophosphonate (**17**). This necessity is likely due to the reversible interaction between Tf_2O and the $-COCH_3$. However, when the α position of the benzyl derivatives was substituted with a −Ph (**23**), a significantly lower conversion of 52% was obtained, possibly due to increased steric hindrance.

In addition to benzyl derivatives, we also investigated naphthyl (**22**), thiophene (**24**) and phenyl (**25**) substrates, all of which provided good fluorination yields. Furthermore, highly functionalized substrates derived from FPND derivative (**26**), Flurpiridaz (**27**), and Socticlestat (**28**), which feature aromatic heterocycles and lactams, were

https://doi.org/10.1038/s41467-024-54208-y

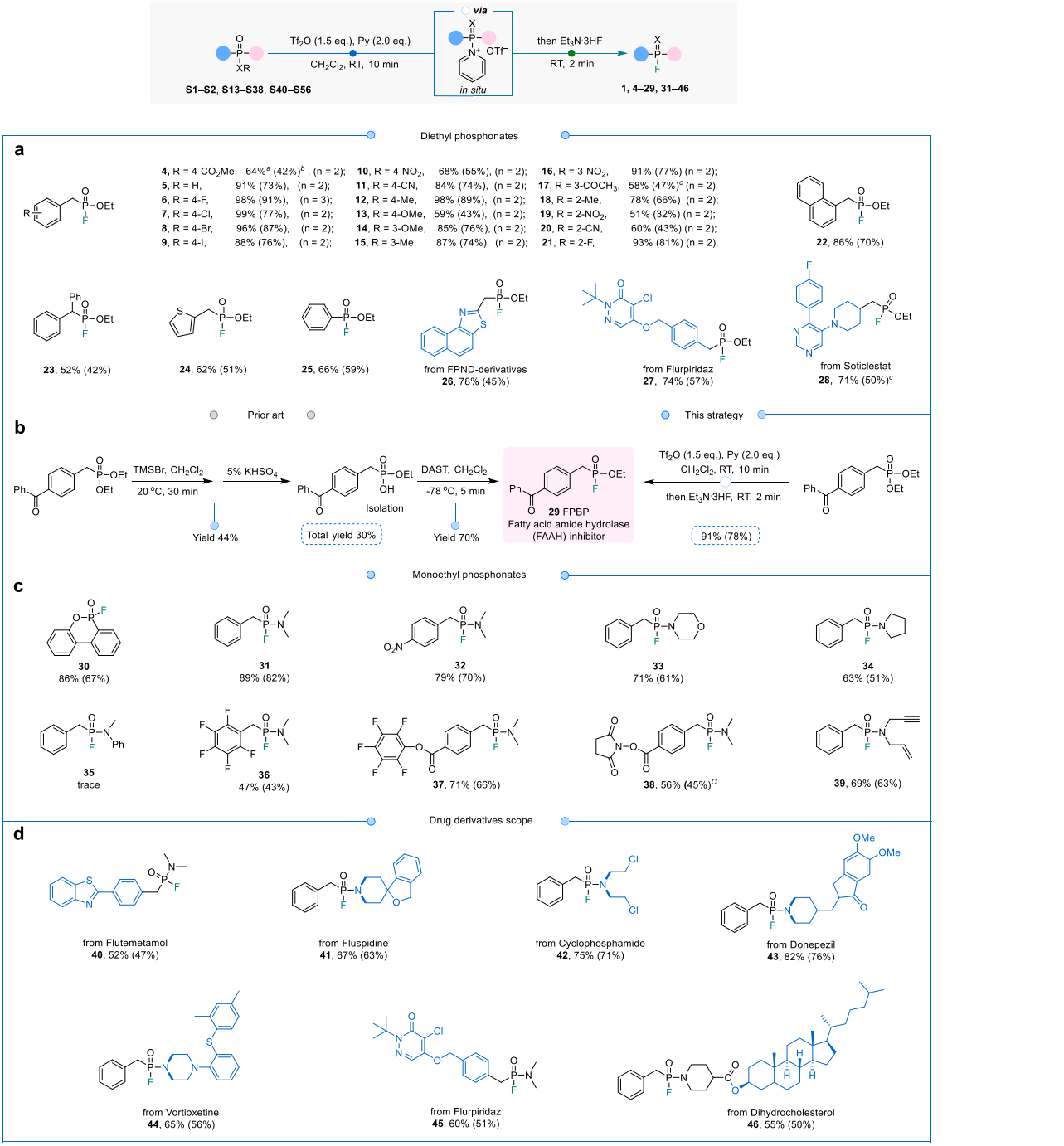

Fig. 5 | Substrate scope for late-stage fluorination of alkyl phosphonates via electrophilic activation. a Fluorination of diethyl phosphonates. [a]Conversions determined by ^{31}P NMR. [b]Isolated yield. [c]Tf_2O (3.0 eq.), Py (4.0 eq.). **b** An exemplification of the method's application in the synthesis of FPBP, a fatty acid amide hydrolase inhibitor. **c** Fluorination of monoethyl phosphonates. **d** Late-stage fluorination of alkyl phosphonates derived from drug molecules.

successfully fluorinated with conversions ranging from 71% to 78%. Importantly, our strategy enabled the one-pot synthesis of 4-(benzoylbenzyl)fluorophosphonic acid ethyl ester (FPBP, **29**), a fatty acid amide hydrolase inhibitor, from the same starting material. This method achieved a high isolated yield of 78% within just 12 min, in contrast to the previous three-step process that required intermediate isolation and utilized the potentially hazardous fluorination reagent DAST, which yielded only 30% (Fig. 4b)[48]. To the best of our knowledge, this work demonstrates the late-stage selective fluorination of alkyl phosphonates to convert P^V–OEt to P^V–F for the construction of fluorophosphines.

The structural diversity of monoethyl phosphonate and its derived drug molecules or functional linker substrates was explored. These entities exhibited various structures and incorporate multiple functional groups that could potentially impact the P–F bond formation process. An ethylphosphonate lactone **30** can be well fluorinated with a good conversion of 86%. Subsequently, the conversion of different secondary amine substituents, such as dimethylamine, morpholine amine and tetrahydropyrrole substituted benzylphosphonamide monoethyl substrate can also be carried out smoothly (**31**–**34**), with conversions ranging from 63% to 89%. However, when *N*-methylaniline group was introduced, the strategy failed

https://doi.org/10.1038/s41467-024-54208-y

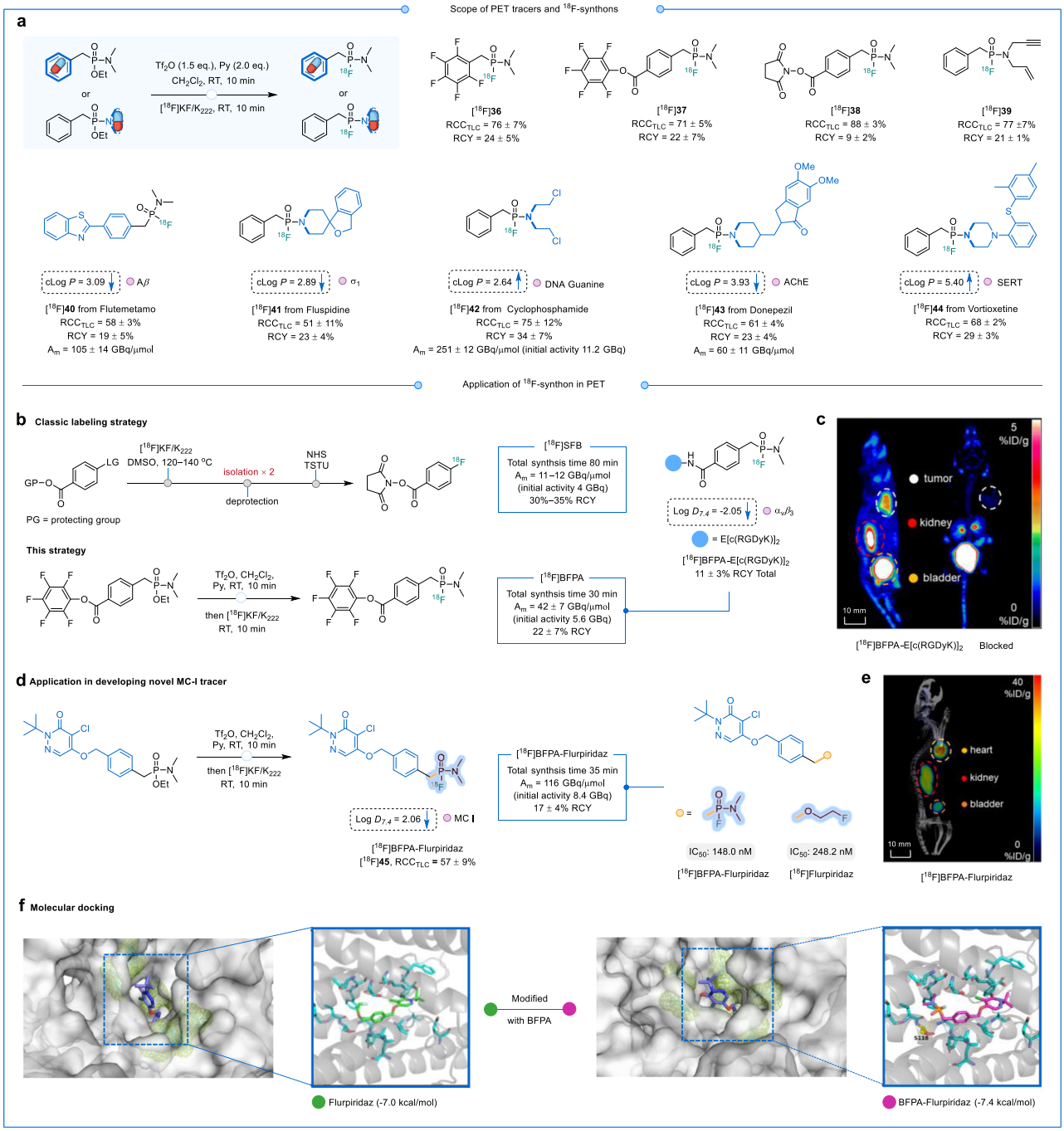

Fig. 6 | PET tracers and ^{18}F-synthons synthesized by late-stage radiofluorination of alkyl phosphonates. a Late-stage radiofluorination of PET tracers and ^{18}F-synthons. RCC_{TLC} determined by radio-TLC ($n = 3$); RCY = isolated ^{18}F-product activity amount/starting amount of radioactivity (decay corrected). cLog *P* values were predicted using ALOGPS 2.1 (http://www.vcclab.org/lab/alogps). Blue arrows pointing upward indicate an increase in cLog *P*/Log $D_{7.4}$ compared to the parent compound, while downward arrows indicate a decrease. The small pink ball after cLog *P*/Log $D_{7.4}$ represents the target of the parent compound. **b** Preparation $\alpha_v\beta_3$ integrin receptor developer [^{18}F]BFPA-E[c(RGDyK)]$_2$. **c** MicroPET images of [^{18}F]BFPA-E[c(RGDyK)]$_2$ in U87MG xenograft mice at 30 min after tail vein injection. 200 μg of E[c(RGDyK)]$_2$ was used to block the tumor uptake of [^{18}F]BFPA-E[c(RGDyK)]$_2$. The white circle is the tumor area. **d** Preparation of PET tracer [^{18}F]BFPA-Flurpiridaz targeting MC I. **e** MicroPET/CT images of healthy mice [^{18}F]BFPA-Flurpiridaz 60 min after caudal vein injection. **f** Molecular Docking. Flurpiridaz and BFPA-Flurpiridaz to MC I (PDB: 7ZM8). Cyan: residues composing the substrate-binding cavity; yellow: residues forming hydrogen bonds; yellow dashed lines: locations of hydrogen bond.

to generate the desired product **35**, since the phenyl (−Ph) group acts as an electron-withdrawing group in *N*-methylaniline, which can reduce the nucleophilicity of O, possibly accounting for the hindrance encountered by O in attacking Tf_2O. Furthermore, several monoethyl phosphinamide-derived substrates with bifunctional linkers (**36**–**39**) can be directly synthesized into the corresponding fluorophosphine derivatives in late-stage process with yields of 43–66%, offering an advantageous approach for synthesizing challenging structures that are typically difficult to access using existing methods. Notably, certain drug molecules derived from monoethyl phosphonate (**40**–**46**), such as nitrogen mustard, flutemetamol, fluspidine, vortioxetine, flurpiridaz and cholestanol, undergo rapid

and highly selective late-stage one pot fluorination under mild conditions, resulting in yields of up to 76%.

Condition optimazation for late-stage ^{18}F-fluorination of alkyl phosphonates

The most commonly used [^{18}F]Fluoride ([^{18}F]F^-) was employed as a default fluoride source for ^{18}F-fluorination. The transition from F^- to [^{18}F]F^- necessitates a reevaluation of the fluoride source and reaction time. A high A_m [^{18}F]F^- aqueous solution is obtained through proton bombardment of [^{18}O]H_2O, followed by elution of [^{18}F]F^- using tetrabutylammonium bicarbonate/Cs_2CO_3 to obtain [^{18}F]TBAF/[^{18}F]CsF or potassium carbonate complexed with the amine-poly-ether crown ligand Kryptofix 222/18-crown-6, resulting in the formation of [^{18}F]KF/K_{222} or [^{18}F]KF/18-crown-6. Among these systems, [^{18}F]KF/K_{222} exhibited the most significant impact on the fluorination of [^{18}F]**1** synthesis (Table S2). We optimized the precursor loading and reaction time to achieve an optimal radiochemical conversion (RCC_{TLC}) of 62 ± 3% (Table S3). Furthermore, we have observed the *P*-benzyl fluorophosphonamide to possess excellent stability under both in vitro and in vivo conditions, suggesting its potential utilization in PET tracer development upon successful ^{18}F-labeling. With the optimal ^{18}F-fluoride source identified, our focus shifted towards assessing the applicability of this approach across a range of tracer and synthon substrates.

Design and synthesis of alkyl phosphonate precursors for ^{18}F-tracers

The design principle for the alkyl phosphonate precursor of a radiotracer is rooted in subtle structural adjustments to a primary compound, ensuring the preservation of its core activity or function. Alkyl fluorophosphonamide is typically incorporated into the lead compound using an 'embedded' strategy as an ^{18}F-building block. Considering that nitrogen-containing active pharmaceuticals make up 85% of the market[49], this adaptability is essential. The amino group of the ethyl *P*-benzyl phosphonamidate building block can align with the amino group in the lead compound (e.g., cyclophosphamide). This enables the rapid construction of the precursor through the reaction of the amino lead compound with readily available ethyl benzylphosphonochloridate. Furthermore, the phosphonamide is a bioisostere of amide, containing a secondary amide moiety in the original molecule (e.g., vortioxetine). The precursor can be formed by reacting an amino-carrying lead compound with ethyl benzylphosphonochloridate. Similarly, the benzyl in ethyl *P*-benzyl phosphonamidate can also originate from the phenyl or benzyl in the lead compound (e.g., Flurpiridaz derivative that targets mitochondrial complex I (MC I)). More importantly, alkyl fluorophosphonamide favorable water solubility contributes to its excellent pharmacokinetic properties. By using the Arbuzov reaction, the corresponding halide compound was converted to diethyl benzylphosphonate derivative, and then subjected to amidation to obtain the precursor.

Late-stage ^{18}F-fluorination of ^{18}F-synthons

The classical method for preparing *N*-succinimidyl-4-[^{18}F]fluorobenzoate ([^{18}F]SFB) requires three-step of synthesis and two isolations, with a total radiosynthesis time of 80 min and an A_m of 11–12 GBq/μmol[50]. In contrast, our phosphonamidic fluoride synthon ([^{18}F]BFPA, [^{18}F]**37**) offers a more efficient approach, as it can be synthesized from ~5.6 GBq [^{18}F]F^- at room temperature with a total radiosynthesis time of 30 min, yielding an A_m of 42 ± 7 GBq/μmol (Fig. 6b). The activated ester [^{18}F]**38**, amenable for amine-specific coupling, delivered 9 ± 2% RCYs. Moreover, the thiol-specific coupling with pentafluorobenzene [^{18}F]**36** provided 24 ± 5% RCYs. The bifunctional synthon [^{18}F]**39**, suitable for alkyne-azide cycloaddition, provided 21 ± 1% RCYs.

When the precursor structure contains electron-rich functional groups—such as amino, carboxyl, hydroxyl, or amide groups—that are incompatible with electrophilic activation conditions, a two-step strategy can be employed to achieve ^{18}F-labeling through [^{18}F]BFPA. [^{18}F]BFPA was readily employed to facilitate the ^{18}F-labeling of the integrin $\alpha_v\beta_3$-targeting peptide E[c(RGDyK)]$_2$, yielding [^{18}F]BFPA-E[RGDyk]$_2$ with RCYs of 11 ± 3% in >99% radiochemical purity (RCP). As depicted in Fig. 6c, at 30 min after injection, U87MG xenografted mice (glioma) exhibited significant tumor-specific uptake of [^{18}F]BFPA-E[RGDyk]$_2$ (RCP > 99%). When blocked by E[c(RGDyK)]$_2$, tumor uptake was substantially reduced from 3.3 ± 0.2 %ID/g (injected dose per gram) to 0.8 ± 0.2 %ID/g. [^{18}F]BFPA-E[RGDyk]$_2$ showed superior in vivo stability in blood, maintaining 94% stability at 60 min post-intravenous administration (Fig. S38d), compared to 74.2% for the NHS-modified ^{18}F-FPRGD2[51]. Additionally, the [^{18}F]BFPA-modified tracers exhibited faster background clearance within 30 min than the [^{18}F]DBPOF-modified tracers.

Late-stage ^{18}F-fluorination of ^{18}F-tracers

Building upon the *P*-benzyl fluorophosphonamide scaffold, we designed and developed ^{18}F-tracers [^{18}F]**40**–[^{18}F]**45** (Fig. 6a). Drug-derived alkyl phosphonates were also subjected to late-stage ^{18}F-fluorination under mild conditions. The RCYs for the flutemetamol derivative [^{18}F]**40**, designed to target amyloid-β (Aβ), and the fluspidine derivative [^{18}F]**41**, targeting σ_1 receptors, were 19 ± 5% and 23 ± 4%, respectively. Furthermore, molecular docking studies revealed that the modified drug molecules can effectively bind in the same structural domain as their parent compounds[52–54], In some cases, the introduction of P=O led to additional hydrogen bonding (as shown in Fig. S40c, d, e, f), resulting in both a lower binding energy—typically reduced by 0.4–1.0 kcal/mol—and a decreasing cLog *P* value[55].

Iterative optimization, guided by the outcomes of non-radioactive reactions, has culminated in the development of an automated method for radiopharmaceutical synthesis. For (pre)clinical applications, the automation of radiosynthesis is crucial (Fig. S32). Employing an AllinOne automated synthesis module enabled the radiosynthesis of the cyclophosphamide derivative [^{18}F]**42**, which was tailored to target DNA guanine. The automated process allowed for the use of higher starting activities (an initial activity of 11.2 GBq), leading to an approximately tenfold increase in A_m (251 ± 12 GBq/μmol, $n = 3$). Additionally, the achieved RCY was 34 ± 7%, with the entire synthesis completed in a significantly shorter time frame. While ^{18}F/^{19}F-isotope exchange facilitated direct ^{18}F-labeling of highly functionalized peptides in one step, a significant limitation was the inseparability of the precursors from the ^{18}F-product, resulting in an A_m of only 2.22–4.81 GBq/μmol[12]. The labeling method described in this study demonstrates the potential to enhance the A_m by nearly 100-fold. Additionally, tracer [^{18}F]**43** derived from donepezil (targeting AChE) and tracer [^{18}F]**44** derived from vortioxetine (targeting serotonin transporter) achieved RCYs of 23 ± 4% and 29 ± 3%, respectively.

The incorporation of phosphine oxide (P=O) as an atypical hydrogen bond acceptor has proven instrumental in achieving the requisite potency and metabolic stability[56]. In the context of myocardial perfusion PET imaging, minimizing uptake in adjacent organs such as lung and liver is essential to provide high imaging contrast with clinical diagnostics. To address this issue, [^{18}F]BFPA-Flurpiridaz (Log $D_{7.4} = 2.06$) with a *P*-benzyl fluorophosphonamide motif integrated into the structure of Flurpiridaz (Log $P = 2.73$)[57] was developed to reduced liver uptake. Subsequent IC_{50} assays affirmed that BFPA-Flurpiridaz (148.0 nM) exhibits a higher affinity compared to Flurpiridaz (248.2 nM) (Section 2.5.2 in the Supplementary Information). In vivo PET imaging in healthy mice showed high specific myocardial uptake of the tracer at 60 min post-intravenous injection, providing clear delineation between the heart and surrounding organs (Fig. 6e). The binding free energy of BFPA-

Flurpiridaz with the MC I protein (PDB: 7ZM8) was found to be −7.4 kcal/mol, compared to −7.0 kcal/mol for Flurpiridaz (Fig. 6f). This suggests that the binding affinity of the tracer is slightly higher than that of the original drug after the incorporation of BFPA. This increased affinity is likely due to the introduction of the P=O moiety, which enables the formation of an additional hydrogen bond with residue S118.

Discussion

In conclusion, a method for the late-stage fluorination of alkyl phosphonates by F^- was presented. Highly electrophilic P^V species have been generated from alkyl phosphonates through a sequential activation strategy of Tf_2O and Py, which were subsequently reacted with F^- to obtain the corresponding P–F bond-containing compounds. Through the combination of controlled experiments and theoretical calculations, the underlying reconfiguration of chemical bonds was revealed, and the fluorination mechanism was thoroughly elucidated, increasing the comprehensibility of our reaction while also providing possibilities for other synthetic designs based on this strategy. This strategy enables direct conversion of alkyl phosphonates from P–XR (R = alkyl) to P–F bonds in the late-stage. A series of ethyl benzylphosphonofluoridates and some fluorophosphines derivatives of drugs were successfully synthesized. Particularly, significant improvements were made regarding the synthesis of FPBP, which previously required a multi-step approach. The method was also employed in ^{18}F-fluorination to synthesize a series of ^{18}F-tracers and synthons derived from benzyl fluorophosphonamide, resulting in the successful development of a [^{18}F]BFPA with a high A_m and exhibiting in vivo stability as an ^{18}F-synthon. Furthermore, our research endeavors extended to the conceptualization and development of [^{18}F]BFPA-Flurpiridaz, a myocardial perfusion imaging agent that exhibits considerable clinical promise, leveraging the favorable pharmacokinetic effects embedded in its structural design. In many instances, the incorporation of the building block into the targeted molecule facilitated a late-stge nucleophilic substitution of the ^{18}F-labeling through this strategy, offering a compelling tool for the ongoing development of PET tracers. Specifically, integrating the P=O skeleton is foreseen as an innovative and effective strategy for reducing the Log *P* of drugs and augmenting affinity.

Methods

General procedure for alkyl phosphates fluorination

Alkyl phosphonates (0.2 mmol) was dissolved in 1 mL CH_2Cl_2 at RT, and then Tf_2O (0.3 mmol, 50.5 µL, 1.5 eq.) was added to the reaction mixture for 5 min, followed by Py (0.4 mmol, 32 µL, 2.0 eq.) for an additional 5 min. Following this, the fluorinating reagent $Et_3N{\cdot}3HF$ (0.5 eq.) was introduced into the system. The progress of the reaction was monitored using TLC or ^{31}P NMR, and after 2 min, the reaction was completed. The reaction mixture, with a volume of approximately 1 mL, underwent direct purification through silica gel column chromatography to afford the desired products.

General procedure for alkyl phosphates radiofluorination

All ^{18}F-labeling reactions were performed following the specified protocol: 3.0 µmol of precursor were dissolved in 300 µL CH_2Cl_2. Then, 2.0 eq. of Tf_2O were added for 5 min, followed by the addition of 1.5 eq. of Py for another 5 min. The resulting intermediate solution was subsequently divided into three equal portions and introduced into separate glass vial reactors, each containing pre-prepared 37–55.5 MBq dried [^{18}F]KF/K_{222}. The reactors were continuously oscillated at RT for 10 min. Upon completion of the reaction, 9900 µL of water was added to quench the reaction. The RCCs of the reaction were determined using radio-TLC with methanol as the developing agent ($n = 3$). The resulting reaction mixture was then subjected to simple purification using a Sep-Pak® Plus Short C18 cartridge (Waters, Part No. WAT020515), followed by separation and purification on a SEP Basic-C18 semi-preparative column (120 A 5 µm 10 × 250 mm). The traces for each radiolabelled product are detailed in Supplementary Section 2.3.3. The desired ^{18}F-products were confirmed via co-injection of the purified ^{18}F-labelled species and reference compound.

Stability evaluation

Purified [^{18}F]BFPA-E[c(RGDyK)]$_2$ and [^{18}F]BFPA-Flurpiridaz were dried under N_2 at room temperature and reconstituted with ultrapure H_2O to achieve an activity of 1–3 MBq/100 µL. Then, 10 µL of [^{18}F]BFPA-E[c(RGDyK)]$_2$ or [^{18}F]BFPA-Flurpiridaz was added to 90 µL of mouse serum, and the mixture was incubated at 37 °C for 60 min, respectively. After adding 100 µL of CH_3CN and vigorously vortexing to generate flocculent precipitate, the supernatant was collected after centrifugation at 7043 × g for 8 min. The supernatant was filtered through a 0.22 µm micropore filter, and the RCP of the filtrate was analyzed by radio-HPLC. Subsequently, the purified [^{18}F]BFPA-E[c(RGDyK)]$_2$ and [^{18}F]BFPA-Flurpiridaz (0.1–0.3 MBq, 10 µL) were dissolved in 90 µL of saline and then incubated at 37 °C for 60 min, respectively. The RCP was determined by radio-HPLC. To evaluate the in vivo metabolic stability of [^{18}F]BFPA-E[c(RGDyK)]$_2$, administer 30–37 MBq intravenously via the tail vein. After 60 min, collect blood and urine samples. Process the samples by adding 100 µL of CH_3CN, mixing thoroughly, and centrifuging. Subsequently, filter the supernatant and analyze it using radio-HPLC to assess metabolic stability.

Cell culture

Cells H9C2 (A cardiomyocyte line derived from rat embryonic heart tissue), purchased from Cell Cook, are maintained, incubated, and washed using a cardiomyocyte-specific modified DMEM medium. In a 24-well plate, seed 10^5 H9C2 cells per well and add 1 mL of complete growth medium to each well. The glioma cell line U87MG was obtained from the China Center for Type Culture Collection of the Chinese Academy of Sciences. The cells were cultured in Leibovitz L15 medium supplemented with 10% (v/v) heat-inactivated fetal bovine serum and penicillin/streptomycin (each at a concentration of 100 U/mL). All cells were regularly tested for mycoplasma contamination and cultured or incubated (as in cell-based assays) in a 5% CO_2 incubator at 37 °C.

IC_{50} determination via cell competitive binding assay

To determine the IC_{50}, cells were incubated in a cell culture incubator overnight until they adhered and nearly covered the wells. Following this, the cells were washed twice with pre-chilled PBS to remove any residual medium. A solution of BFPA-Flurpiridaz or Flurpiridaz (concentrations ranging from 10^{-12} M to 10^{-4} M) was added to each well at a volume of 100 µL, and the cells were incubated for 10 min to evaluate their inhibitory effects on [^{18}F]Flurpiridaz uptake in H9C2 cells, with four replicate wells established for each concentration to ensure reliability. Afterward, 400 µL of a radioactively labeled sample with a specific activity of 0.37 MBq was added to each well, and the cells were incubated for an additional 60 min. Once incubation was complete, the medium was completely aspirated, and each well was washed twice with 0.5 mL of pre-chilled PBS containing 0.2% BSA to remove any unbound label. Then, 1 mL of 1 M NaOH solution was added to each well, followed by a 5–10 min incubation period. The cells were gently dislodged and scraped from the bottom of the wells using a pipette, and all liquid and cells were transferred into a marked plastic tube. Three aliquots of the labeled medium were taken from the tube to serve as standard samples. Finally, the radioactivity count of all samples was measured using a γ-counter (WIZARD^2 2480), and data processing, graphing, and calculation of cellular probe uptake at various time points were performed using Graphpad Prism 8.2.1. Detailed data processing can be found in Supplementary Information 2.5.2.

Molecular docking

In the molecular docking study, AutoDock Vina 1.2.0 was employed to dock two ligands—the parent drug molecule and its BFPA-modified derivative—onto the target protein. For each ligand, the most favorable binding conformation was selected based on the docking score and the plausibility of the interaction.

Octanol/water partition coefficient (Log $D_{7.4}$)

The log $D_{7.4}$ values of [^{18}F]BFPA-Flurpiridaz and [^{18}F]BFPA-E[c(RGDyK)]$_2$ in the octanol/water system were determined. Briefly, 100 μL of the radiotracer solution was diluted with 1 mL PBS (0.15 M, pH 7.4) and 0.9 mL octanol, vortexed for 5 min, and centrifuged at 7043 × g for 5 min. For [^{18}F]BFPA-Flurpiridaz, a 100 μL aliquot of the organic phase was transferred to a fresh mixture of 0.9 mL octanol and 1 mL PBS for further vortexing and centrifugation. For [^{18}F]BFPA-E[c(RGDyK)]$_2$, a 100 μL aliquot of the aqueous phases was transferred. Radioactivity in the organic and aqueous phases (100 μL) was measured using a γ-counter. All experiments were performed in triplicate, with results reported as mean ± SD. cLog P values were predicted using ALOGPS 2.1 (http://www.vcclab.org/lab/alogps).

Animal

All the animal experiments were carried out in accordance with the Instructions of Laboratory Animal Ethics Committee of Xiamen University (240506 XMULAC20240099).

Nude mice (4–8 weeks old) and male BALB/c mice (7–8 weeks old) were purchased from Xiamen University Laboratory Animal Center. The mice were housed in the Laboratory Animal Center of Xiamen University under a 12-h light/dark cycle at 22 ± 2 °C and 40–60% humidity.To establish U87MG tumor-bearing mice, U87MG cells were injected subcutaneously into the right forelimb of 4 to 8-week-old nude mice (5×10^6 in 100 μL PBS). The mice were used for tumor imaging studies when the tumor size reached 100–150 mm^3 (2–3 weeks post-inoc ulation).

PET/CT imaging

All MicroPET/CT images were acquired using an Inveon MicroPET/CT scanner (Siemens) and subsequently analyzed with the Inveon Research Workplace 4.2 (Siemens). For the MicroPET imaging study, mice received a bolus tail-vein injection of a solution of ^{18}F-tracer (~3.7 MBq) dissolved in 0.9% saline (100 μL). The mice were anesthetized with inhaled 2% isoflurane continuously for 5 min before imaging and then positioned on the MicroPET/CT scanner bed for a 5-min PET scan.

Reporting summary

Further information on research design is available in the Nature Portfolio Reporting Summary linked to this article.

Data availability

The authors declare that the data supporting the findings of this study are available within the Article and its Supplementary Information Files or from the corresponding author upon request. Source data are provided with this paper.

References

1. Jang, Y. J., Kim, K., Tsay, O. G., Atwood, D. A. & Churchill, D. G. Update 1 of: destruction and detection of chemical warfare agents. *Chem. Rev.* **115**, PR1–PR76 (2015).
2. Mercey, G. et al. Reactivators of acetylcholinesterase inhibited by organophosphorus nerve agents. *Acc. Chem. Res.* **45**, 756–766 (2012).
3. Worek, F., Wille, T., Koller, M. & Thiermann, H. Toxicology of organophosphorus compounds in view of an increasing terrorist threat. *Arch. Toxicol.* **90**, 2131–2145 (2016).
4. Franca, T. C. C. et al. Novichoks: the dangerous fourth generation of chemical weapons. *Int. J. Mol. Sci.* **20**, 1222 (2019).
5. Caputo, C. B., Houmjet, L. J., Dobrovetsky, R. & Stephan, D. W. Lewis acidity of organofluorophosphonium salts: hydrodefluorination by a saturated acceptor. *Science* **341**, 1374–1376 (2013).
6. Hounjet, L. J., Caputo, C. B. & Stephan, D. W. Phosphorus as a Lewis Acid: CO_2 Sequestration with Amidophosphoranes. *Angew. Chem. Int. Ed.* **51**, 4714–4717 (2012).
7. Pérez, M., Caputo, C. B., Dobrovetsky, R. & Stephan, D. W. Metal-free transfer hydrogenation of olefins via dehydrocoupling catalysis. *Proc. Natl Acad. Sci. USA* **111**, 10917–10921 (2014).
8. Sun, S. et al. Phosphorus fluoride exchange: multidimensional catalytic click chemistry from phosphorus connective hubs. *Chem* **9**, 2128–2143 (2023).
9. Studenov, A. R., Adam, M. J., Wilson, J. S. & Ruth, T. J. New radiolabelling chemistry: synthesis of phosphorus–[^{18}F]fluorine compounds. *J. Label. Compd. Radiopharm.* **48**, 497–500 (2005).
10. Vabre, B. et al. Radiofluorination of a NHC–PF_5 adduct: toward new probes for ^{18}F PET imaging. *Chem. Commun.* **53**, 8657–8659 (2017).
11. Jiang, H. & DeGrado, T. R. [^{18}F]Tetrafluoroborate ([^{18}F]TFB) and its analogs for PET imaging of the sodium/iodide symporter. *Theranostics* **8**, 3918–3931 (2018).
12. Hong, H. et al. Rapid one-step ^{18}F-radiolabeling of biomolecules in aqueous media by organophosphine fluoride acceptors. *Nat. Commun.* **10**, 989 (2019).
13. Mou, Z. et al. Nucleophilic ^{18}F-fluorination of phosphorofluoridates and phosphonofluoridic acids via imidazole-activated precursors. *Tetrahedron Lett.* **68**, 152917 (2021).
14. Tang, X., Lv, S., Mou, Z., Liu, X. & Li, Z. Cu(II)-Mediated direct ^{18}F-dehydrofluorination of phosphine oxides in high molar activity. *EJNMMI Radiopharm. chem.* **9**, 4 (2024).
15. Yang, H. et al. Simplified one-pot ^{18}F-labeling of biomolecules with in situ generated fluorothiophosphate synthons in high molar activity. *Theranostics* **13**, 472–482 (2023).
16. Li, Z. et al. Surfactants accelerate isotope exchange-based ^{18}F-Fluorination in water. *Langmuir* **39**, 9007–9016 (2023).
17. Corriu, R. J. P. et al. Silicon phosphorus analogies. Fluoride activation of nucleophilic displacement at the tetrahedral phosphorus: an example of nucleophilic assistance to nucleophilic substitution. *J. Am. Chem. Soc.* **106**, 1060–1065 (1984).
18. Janssen, A. P. A. et al. Development of a multiplexed activity-based protein profiling assay to evaluate activity of endocannabinoid hydrolase inhibitors. *ACS Chem. Biol.* **13**, 2406–2413 (2018).
19. Timperley, C. M., Arbon, R. E., Saunders, S. A. & Water, M. J. Fluorinated phosphorus compounds: Part 6. The synthesis of bis(-fluoroalkyl) phosphites and bis(fluoroalkyl) phosphorohalidates. *J. Fluor. Chem.* **113**, 65–78 (2002).
20. Gupta, H. K., Pardasani, D., Mazumder, A., Purohit, A. K. & Dubey, D. K. Tetrabutylammonium tetra (*tert*-butyl alcohol) coordinated fluoride-an efficient reagent for the synthesis of fluorine derivatives of phosphorus(V) compounds. *Tetrahedron Lett.* **50**, 2697–2699 (2009).
21. Liu, N., Mao, L.-L., Yang, B. & Yang, S.-D. Copper-promoted oxidative-fluorination of arylphosphine under mild conditions. *Chem. Commun.* **50**, 10879–10882 (2014).
22. Purohit, A. K. et al. A single-step one pot synthesis of dialkyl fluorophosphates from dialkylphosphites. *Tetrahedron Lett.* **56**, 4593–4595 (2015).
23. Li, Q.-W. et al. TFAA/DMSO-Promoted Fluorination of P(O)–H and P(O)–OH compounds: compatible access to Fluorophosphonates and Phosphonofluoridates. *Adv. Synth. Catal.* **364**, 938–946 (2022).
24. Chen, Q. et al. Electrophilic Fluorination of secondary Phosphine Oxides and its application to P–O bond construction. *J. Org. Chem.* **81**, 10043–10048 (2016).

25. Bigley, A. N., Harvey, S. P., Narindoshvili, T. & Raushel, F. M. Substrate analogues for the Enzyme-Catalyzed detoxification of the Organophosphate nerve agents—Sarin, Soman, and Cyclosarin. *Biochemistry* **60**, 2875–2887 (2021).
26. Chworoś, A. & Woźniak, L. A. A Facile conversion of Thio- and Selenophosphoric acids and their derivatives into Fluoridates by means of reaction with Silver Fluoride. *Tetrahedron Lett.* **40**, 9337–9340 (1999).
27. Lopusiński, A. Chemistry of *S*-trifluoromethyl organophosphorothioates and their steructural analogs a convenient synthesis of organophosphorus fluoridates. *Phosphorus, Sulfur Silicon Relat. Elem.* **45**, 137–143 (1989).
28. Guo, L., Auarez, A. I., Braden, M. R., Gerdes, J. M. & Thompson, C. M. Inhibition of acetylcholinesterase by chromophore-linked fluorophosphonates. *Bioorg. Med. Chem. Lett.* **20**, 1194–1197 (2010).
29. Tully, S. E. & Cravatt, B. F. Activity-based probes that target functional subclasses of phospholipases in proteomes. *J. Am. Chem. Soc.* **132**, 3264–3265 (2010).
30. Zhao, S. et al. Deoxyfluorination of carboxylic, sulfonic, phosphinic acids and phosphine oxides by perfluoroalkyl ether carboxylic acids featuring CF_2O units. *Chin. J. Chem.* **39**, 1225–1232 (2021).
31. Miller, L. P., Vogel, J. A., Harel, S., Krussman, J. M. & Melvin, P. R. Rapid generation of P(V)–F bonds through the use of sulfone iminium fluoride reagents. *Org. Lett.* **25**, 1834–1838 (2023).
32. Łopusiński, A. & Michalski, J. Novel application of Sulfonyl Chloride Fluoride in the synthesis of Organophosphorus Fluorine Compounds: direct conversion of and groups into groups. *Angrew. Chem. Int. Ed.* **21**, 294 (1982).
33. Zhang, G.-F., Han, L.-J., Guan, C.-F. & Ding, C.-R. SO_2F_2-mediated Fluorination of P(O)–H and P(O)–OH compounds under mild conditions. *J. Org. Chem.* **88**, 13142–13148 (2023).
34. Wang, C. et al. Direct ^{18}F-labeling of biomolecules via spontaneous site-specific nucleophilic substitution by F^- on phosphonate prostheses. *Org. Lett.* **23**, 4261–4266 (2021).
35. Preshlock, S., Tredwell, M. & Gouverneur, V. ^{18}F-labeling of arenes and heteroarenes for applications in positron emission Tomography. *Chem. Rev.* **116**, 719–766 (2016).
36. Fañanás-Mastral, M. & Feringa, B. L. Copper-catalyzed synthesis of mixed Alkyl Aryl phosphonates. *J. Am. Chem. Soc.* **136**, 9894–9897 (2014).
37. Huang, H., Denne, J., Yang, C.-H., Wang, H. & Kang, J. Y. Direct Aryloxylation/Alkyloxylation of Dialkyl phosphonates for the synthesis of mixed phosphonates. *Angew. Chem. Int. Ed.* **57**, 6624–6628 (2018).
38. Adler, P. et al. Chemoselective activation of diethyl phosphonates: modular synthesis of biologically relevant phosphonylated scaffolds. *Angew. Chem. Int. Ed.* **57**, 13330–13334 (2018).
39. Clarak, J. H. Fluoride Ion as a base in organic synthesis. *Chem. Rev.* **80**, 429–452 (1980).
40. Tang, Z., Mo, K., Ma, X., Huang, J. & Zhao, D. *para*-selective Radical Trifluoromethylation of Benzamide Derivatives via Iminium Intermediates. *Angew. Chem. Int. Ed.* **61**, 1–7 (2022).
41. Hagiwara, H., Watanabe, N., Ijuin, H. K., Yamada, M. & Matsumoto, M. Synthesis of bicyclic Dioxetanes bearing a 4-(Benzimidazol-2-yl) –3-hydroxyphenyl group and their base-induced Chemiluminescent decomposition in an aprotic medium and in an aqueous medium. *Heterocyclics* **87**, 65–78 (2013).
42. Leclercq, L., Suisse, I., Nowogrocki, G. & gbossou-Niedercorn, F. Halide-free highly-pure imidazolium triflate ionic liquids: preparation and use in palladium-catalysed allylic alkylation. *Green. Chem.* **9**, 1097–1103 (2007).
43. Huang, H. & Kang, J. Y. Triflic anhydride (Tf_2O)-activated transformations of amides, sulfoxides and phosphorus oxides via nucleophilic trapping. *Synthesis* **54**, 1157–1202 (2022).
44. Baraznenok, I. L., Nenajdenko, V. G. & Balenkova, E. S. Chemical transformations induced by Triflic Anhydride. *Tetrahedron* **56**, 3077–3119 (2000).
45. Michaelis, A. & Kaehne, R. The reaction of alkyl iodides with phosphites. *Chem. Ber.* **31**, 1048–1058 (1898).
46. Ozturk, T., Ertas, E. & Mert, O. Use of Lawesson's Reagent in Organic Syntheses. *Chem. Rev.* **107**, 5210–5278 (2007).
47. Barthen, P., Frank, W. & Ignatiev, N. Development of low viscous ionic liquids: the dependence of the viscosity on the mass of the ions. *Ionics* **21**, 149–159 (2015).
48. Patricelli, M. P. & Cravatt, B. F. Characterization and manipulation of the Acyl chain selectivity of fatty acid amide hydrolase. *Biochemistry* **40**, 6107–6115 (2001).
49. Heravi, M. M. & Zadsirjan, V. Prescribed drugs containing nitrogen heterocycles: an overview. *RSC Adv.* **10**, 44247–44311 (2020).
50. Vaidyanathan, G. & Zalutsky, M. R. Synthesis of *N*-succinimidyl 4-[^{18}F]fluorobenzoate, an agent for labeling proteins and peptides with ^{18}F. *Nat. Protoc.* **1**, 1655–1661 (2006).
51. Wu, Z. et al. ^{18}F-labeled mini-PEG spacered RGD dimer (^{18}F-FPRGD2): synthesis and microPET imaging of $\alpha_v\beta_3$ integrin expression. *Eur. J. Nucl. Med. Mol. Imaging* **34**, 1823–1831 (2007).
52. Eberhardt, J., Santos-Martins, D., Tillack, A. F. & Forli, S. AutoDock Vina 1.2.0: new docking methods, expanded force field, and python bindings. *J. Chem. Inf. Model.* **61**, 3891–3898 (2021).
53. Trott, O. & Olson, A. J. AutoDock Vina: improving the speed and accuracy of docking with a new scoring function, efficient optimization, and multithreading. *J. Comput. Chem.* **31**, 455–461 (2010).
54. Stierand, K. & Rarey, M. Drawing the PDB-protein-ligand complexes in two dimensions. *ACS Med. Chem. Lett.* **1**, 540–545 (2010).
55. Tetko, I. V. & Tanchuk, V. Y. Application of associative neural networks for prediction of lipophilicity in ALOGPS 2.1 program. *J. Chem. Inf. Comput. Sci.* **42**, 1136–1145 (2002).
56. Finkbeiner, P., Hehn, J. P. & Gnamn, C. Phosphine oxides from a medicinal chemist's perspective: physicochemical and in vitro parameters relevant for drug discovery. *J. Med. Chem.* **63**, 7081–7107 (2020).
57. Nekolla, S. G. et al. Evaluation of the novel myocardial perfusion positron-emission tomography tracer ^{18}F-BMS-747158-02: comparison to ^{13}N-ammonia and validation with microspheres in a pig model. *Circulation* **119**, 2333–2342 (2009).

Acknowledgements

National Natural Science Foundation of China 22476167, 81971674 (Z.L.), the National University of Singapore NUHSRO/2020/133/Startup/08, UHSRO/2023/008/NUSMed/TCE/LOA, NUHSRO/2021/034/TRP/09/Nanomedicine (X.C.), National Medical Research Council MOH-001388-00, MOH-001041, CG21APR1005 (X.C.), Singapore Ministry of Education MOE-000387-00 (X.C.), and National Research Foundation NRF-000352-00 (X.C.). We extend their gratitude to the Theoretical and Computational Chemistry Team from Shiyanjia Lab (www.shiyanjia.com) for their assistance. We would also like to thank J.Y. and X.W. from the School of Public Health at Xiamen University for their help and analysis in molecular docking.

Author contributions

Z.L. conceived the study and coordinated all the research. K.Z. originated the (radio)fluorination of alkyl phosphonates via electrophilic activation. W.F., Z.M. offered help in chemical synthesis and radiolabeling. Computational chemistry was carried out by L.Z., M.M., Z.Z. and X.L. offered help in biology and microPET imaging experiments. Results were collaboratively analyzed, and the manuscript was prepared by Z.L., K.Z. and X.C. All authors participated in research discussions.

Competing interests

The authors declare no competing interests.

Additional information

Supplementary information The online version contains Supplementary Material available at https://doi.org/10.1038/s41467-024-54208-y.

Correspondence and requests for materials should be addressed to Zijing Li.

Peer review information *Nature Communications* thanks Tian-Yu Sun, Zehui Wu and the other, anonymous, reviewers for their contribution to the peer review of this work. A peer review file is available.